Modelling of mass transfer in Taylor flow: Investigation with the PLIF-I technique

C. Butler[a,b], *E. Cid*[a,b], *A.-M. Billet*[a,b,*]

[a] *Laboratoire de Génie Chimique, Université de Toulouse, CNRS, INPT, UPS, Toulouse, France*
[b] *FERMaT, Université de Toulouse, CNRS, INPT, UPS, INSA, Toulouse, France*

A B S T R A C T

An experimental investigation of mass transfer between bubbles, slugs and lubrication films is performed by means of optical techniques for air–water Taylor flows in a 3 mm glass channel. Bubble size, shape and velocity, as well as slug size and film thickness, are measured by use of the shadowgraphy technique. The PLIF-I technique, with associated specific technical adjustments and image processing methods, gives access to the dissolved oxygen concentration in the liquid phase with high spatial and temporal resolutions. Values of concentration are measured in the slugs and, for the first time, in the lubrication films, leading to the quantification of mass transfer contributions from caps and from the central bubble body. Results for overall mass transfer are compared to literature models based on volumetric coefficient k_La. Among them the model proposed by Van Baten and Krishna (2004), which considers cap and film contributions to k_La. They are found to fail to accurately predict the experimental data of average O_2 concentration in the liquid phase for short slugs ($L_s < 2d_c$). An improved version of this model is proposed, allowing calculation of O_2 concentration for films and slugs along the channel. The model needs flow characteristics, which are obtained by shadowgraphy.

Keywords:
Mass transfer
Taylor flow
Lubrication film
PLIF-I
Shadowgraphy
Modelling

1. Introduction

Over the past several years, it has been claimed that structured reactors offer interesting possibilities in the field of chemical reaction engineering. Amongst them, monolith reactors, also known as 'honeycomb reactors', have appeared as a cutting-edge technology for gas–liquid catalytic reactors in regard to conventional reactors, which suffer various drawbacks. These include liquid back-mixing and need for catalyst separation and recycling (in slurry bubble columns), significant attrition of the catalyst (in fluidised-beds), and significant pressure drop and diffusional limitation (in fixed-beds). Monolith reactors have been the focus of considerable study for almost four decades as they promise to overcome these problems. As well as other interesting points (such as low pressure drop, low risk for fouling or clogging and for hot spots), monolith reactors host in their channels specifically tunable gas–liquid flow regimes. One such regime, the so-called Taylor flow (or bubble-train or slug flow) leads to interesting values of interfacial area and of rates of mass transfer (Heiszwolf et al., 2001; Vandu et al., 2005), which is particularly convenient as gas–liquid mass transfer is the limiting phenomenon when fast chemical reactions are involved. The overall volumetric gas–liquid mass transfer coefficient, k_La, was reported to be much larger in monolith reactors operating in the Taylor flow regime (0.1–1 s^{-1}) (Heiszwolf et al., 2001; Vandu et al., 2004) than in stirred tanks (0.03–0.4 s^{-1}), bubble columns (0.005–0.25 s^{-1}) or packed beds (0.004–1 s^{-1}) (Yue et al., 2007). This enhanced mass transfer was attributed to the existence of a thin liquid film (a few tens of μm) laying between the bubble and the channel wall, as well as to the efficient convective mixing within the liquid slugs provided they are short enough (Mehdi et al., 2013). What is more, the lubrication film contribution to mass transfer becomes crucial when a heterogeneous reaction

* *Corresponding author at:* Laboratoire de Génie Chimique, 4 allée Emile Monso, CS 44362, 31030 Toulouse cedex 4, France
E-mail addresses: colin.butler@ensiacet.fr (C. Butler), emmanuel.cid@ensiacet.fr (E. Cid), annemarie.billet@ensiacet.fr (A.-M. Billet).
http://dx.doi.org/10.1016/j.cherd.2016.09.001

occurs at the catalyst coated wall because a sharp concentration gradient is locally generated in this case. So far, empirical correlations for the volumetric (liquid side) mass transfer coefficient, k_La, are available in literature for Taylor flows, but knowledge and understanding of the phenomena occurring at the local scale are still lacking, which could lead to pre-design rules and scaling laws for monolith reactors.

In the present work, mass transfer is investigated at the bubble and slug scale in Taylor flow in a channel of 3 mm of internal diameter, by use of non-invasive techniques with high spatial and temporal resolutions: shadowgraphy and Planar Laser Induced Fluorescence with dye Inhibition (here after PLIF-I). The objectives are (i) to measure dissolved gas concentration values in liquid phase, (ii) to compare them to existing mass transfer models in order to sort those of most relevance, (iii) to quantify lubrication film and bubble cap contributions in an attempt to understand the phenomena taking place, and (iv) to propose an improved model, allowing for the prediction of the dissolved oxygen concentration [O_2] in films and slugs along the channel. This model, based on phenomenological considerations, is intended as a method for fast and easy estimation of gas–liquid mass transfer for pre-design of monolith reactors.

2. State of the art: mass transfer in Taylor flow

2.1. *Experimental investigations*

It was shown that k_La values measured in monolith reactors correlate rather well with those predicted from single-channel models (Heiszwolf et al., 2001; Vandu et al., 2004). Most works on gas–liquid mass transfer have been devoted to single millimetric capillaries (Vandu et al., 2005; Mehdi et al., 2013; Berčič and Pintar, 1997; Irandoust et al., 1992; Van Baten and Krishna, 2004; Shao et al., 2010; Liu and Wang, 2010; Hassanvand and Hashemabadi, 2012; Pan et al., 2014) and the experimental contributions have provided data measured at the inlet and at the outlet of a channel. The relative contributions of bubble caps and lubricating film to the gas–liquid mass transfer have been thoroughly discussed, but conclusions were mainly drawn for non-reactive systems where film saturation with the transferring species may hinder its contribution. No experimental work has yet investigated the specific contributions from lubrication films and from bubble caps and few chemical engineering models have been proposed in literature to take into account those contributions (Hatziantoniou et al., 1986; Nijhuis et al., 2001; Kreutzer et al., 2001).

Recently, non-invasive experimental methods have appeared, allowing fully developed Taylor flows to be successfully studied (Tan et al., 2012; Dietrich et al., 2013; Yao et al., 2014). However, some of these methods are suitable for specific fluid systems only, where chemical reaction and chemical enhancement factor are implied, or are valid for very small reactors only. What is more, these techniques do not permit the investigation of the lubrication film.

2.2. *Existing models for mass transfer in Taylor flows*

As the liquid phase in Taylor flow consists of a train of mixed slugs, it has often been represented, for mass transfer purposes, using the plug flow model (Berčič and Pintar, 1997; Vandu et al., 2005; Shao et al., 2010; Yue et al., 2007). For this kind of model, uniform velocity and concentration are assumed for the liquid phase over the channel cross section, regardless of the actual structure of the flow. A single value of k_La is then used to express mass exchange between gas and liquid phases:

$$u_{TP}\frac{dC}{dz} = k_La[C^* - C(z)] \quad (1)$$

where z is the axial coordinate along the channel, u_{TP} is the total superficial velocity of fluids (gas plus liquid) in the channel, C(z) the current concentration of transferred gas in the liquid phase, and C^* the saturation concentration of dissolved gas in the liquid. Note that a is considered here as the interface surface per unit volume of channel. Eq. (1) can be integrated into:

$$\frac{C(z)}{C^*} = 1 - \left[1 - \frac{C(z=0)}{C^*}\right]\exp\left(-k_La\frac{z}{u_{TP}}\right) \quad (2)$$

Correlations for k_La estimation are found in literature; the major ones (i.e. most often cited) are listed in Table 1. The major advantage of the plug flow model associated with these correlations for k_La is that it can be applied with the knowledge of phase flow rates, channel diameter, fluid properties and bubble and slug lengths only. The Berčič and Pintar (1997) correlation (Eq. (A) in Table 1) was established for long bubbles with almost saturated films. In the correlations from Van Baten and Krishna (2004) (Eqs. (B1) and (B2)), the contributions from caps (left term in equations) and film (right term in equations) to mass transfer are evaluated on the basis of the Higbie penetration mass transfer model and of falling film theory, respectively. Note that conditions of establishment of the correlations proposed by Van Baten and Krishna (2004) correspond to short contact time of the liquid film ($\tau_f < 0.1\delta_f^2/D$). Eq. (B1) uses the exact dimensions of bubble, film and slug, unlike Eq. (B2) where these dimensions are estimated thanks to the operational parameters (for instance film length, L_{f-b}, is estimated from L_{UC} and the ratio of bubble and unit cell volumes), and may lead *a priori* to less accurate results. Vandu et al. (2005) correlated film contribution only, based on the $(k_L)_{f-b}$ suggested by Van Baten and Krishna (2004), where a multiplicative value of 4.5 best fitted the experimental data of air absorption in water in 1–3 mm diameter capillaries of circular and square cross-sections. Eq. (C1) should then be valid for Taylor flows in which film contribution is dominant. Shao et al. (2010) tuned the multiplicative constant in Eq. (C1) to match CFD computed results for the case of CO_2 absorption into an aqueous solution of NaOH. The correlation from Yue et al. (2007) (Eq. (D)) was derived for narrow channels (less than 1 mm) in addition to high gas and liquid superficial velocities ($1\,m/s < u_{TP} < 12\,m/s$).

More recent models take into account the detailed structure of Taylor flow (Abiev, 2013; Kececi et al., 2009; Svetiov and Abiev, 2015). Kececi et al. (2009) derive, for rectangular channels, a theoretical analysis of the recirculation time in the liquid slugs for laminar flow, and proposed a correlation for this characteristic time. Svetiov and Abiev (2015) consider the liquid slug as stratified in three layers: the film at the wall, and the inner and outer layers in the Taylor vortex. For this model, hydrodynamics terms are evaluated from the Poiseuille structure of the liquid flow and from the lubrication film thickness, as correlated in literature (Thulasidas et al., 1997). The mass transfer (or transport) terms are determined from diffusion layer consideration and from annular film theory. This

Table 1 – Correlations from literature for estimation of k_La values (k_La is expressed in s^{-1}, where interfacial a is expressed in m^2 per volume of unit cell).

Authors	Correlation	Eq.
Berčič and Pintar (1997)	$k_La = 0.111\frac{u_{TP}^{1.19}}{[(1-\varepsilon_V)L_{UC}]^{0.57}}$	(A)
Van Baten and Krishna (2004)	$k_La = \frac{2\sqrt{2}}{\pi}\sqrt{\frac{Du_b}{d_c}\frac{4d_b^2}{L_{UC}d_c^2}} + \frac{2}{\sqrt{\pi}}\sqrt{\frac{Du_b}{L_{f-b}}\frac{4d_bL_{f-b}}{d_c^2L_{UC}}}$	(B1)
Van Baten and Krishna (2004)	$k_La = \frac{2\sqrt{2}}{\pi}\sqrt{\frac{Du_b}{d_c}\frac{4}{L_{UC}}} + \frac{2}{\sqrt{\pi}}\sqrt{\frac{Du_b}{\varepsilon_V L_{UC}}\frac{4\varepsilon_V}{d_c}}$	(B2)
Vandu et al. (2005)	$k_La = 4.5\sqrt{\frac{Du_{GS}}{L_{UC}}\frac{1}{d_c}}$	(C1)
Shao et al. (2010)	$k_La = 3\sqrt{\frac{Du_{GS}}{L_{UC}}\frac{1}{d_c}}$	(C2)
Yue et al. (2007)	$Sh_L\, a\, d_c = 0.084Re_G^{0.213}Re_L^{0.912}Sc_L^{0.5}$	(D)

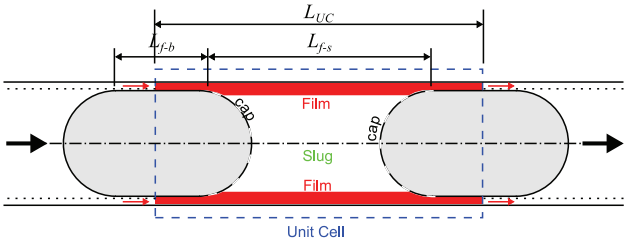

Fig. 1 – Schematic representation of unit cell, bubble, slug and film.

model needs a differential equation in space (2-dimensional) and time to be solved, and could be interestingly compared to experimental results. In a view of fast and easy estimation of gas–liquid mass transfer for pre-design of monolith reactors, this model however requires a significant amount of calculation.

3. Calculation: pre-design model for mass transfer in Taylor flow

As mentioned in Section 2.2, the Van Baten and Krishna (2004) model distinguishes the contributions from films and caps to mass transfer in the unit cell. An overall k_La value is built for the unit cell from 2 contributions:

$$k_La = (k_La)_{caps} + (k_La)_{f-b} \tag{3}$$

where $(k_La)_{caps} = k_{L,caps}a_{caps}$ and $(k_La)_{f-b} = k_{L,f-b}a_{f-b}$. The terms a_{caps} and a_{f-b} are derived in Eq. (B2) in Table 1. The overall k_La value is weighted in Eq. (1) by the average driving concentration difference in the whole unit cell. As a consequence, in this model, actual volumes and concentrations for films and slugs cannot contribute to the calculation of the resulting dissolved oxygen concentration.

In this work, the separate use of the two contributions is preferred. To that purpose, separate slug and film zones are taken into account (see Fig. 1). A channel fed with deoxygenated water and pure O_2 gas bubbles is considered. Focus is made on a unit cell of volume Vol_{UC} and length L_{UC}, travelling along the channel at velocity u_{TP} (Fig. 1). The slug travels at a velocity u_{TP} (Thulasidas et al., 1995) and is assumed to be perfectly mixed. For simplification, it is considered to be the same diameter as the bubble (d_b). The slug reaches the axial position z in the channel at a time instant t defined as:

$$t = \frac{z}{u_{TP}} \tag{4}$$

The slug is fed by mass transfer from the bubble cap surfaces and by mass exchange with the liquid film layer close to the wall. The estimation of mass transfer between bubble and slug is based on the volumetric coefficient $(k_La)_{caps}$ (per volume of unit cell) as expressed by Van Baten and Krishna (2004) (left term in Eq. (B1), Table 1); however u_{TP} is used in this relation instead of u_b: the liquid velocity profile in the slug is known to conform to the Poiseuille law (Svetiov and Abiev, 2015) where u_{TP} is the average velocity in the slugs. For mass exchange between the slug and liquid film layer, we consider that the recirculation in slug meets uniform concentration at film boundary. Following literature analysis of fully-developed laminar flow in a circular channel with a constant boundary concentration (Incropera and DeWitt, 2002; Das, 2010), the assumption is made that $Sh = 3.66$, where Sh is the Sherwood number. The value of Sh is a constant, independent of Re, Sc, and axial location (Incropera and DeWitt, 2002). Therefore, mass exchange between film layer and slug is evaluated on the basis of a volumetric coefficient $(k_L)_{f-s}$, defined as:

$$(k_L)_{f-s} = \frac{3.66D}{d_c} \tag{5}$$

where D is the diffusivity of dissolved gas in the considered liquid.

Defining C_s and C_f as the concentrations of dissolved gas in slug and film at time t (or position z in channel), respectively, a balance equation of dissolved gas in the slug volume Vol_s is then derived over an infinitesimal time instant dt:

$$Vol_s[C_s(t+dt) - C_s(t)] = \{(k_La)_{caps}[C^* - C_s(t)]Vol_{UC} + (k_L)_{f-s}A_{f-s}[C_f(t) - C_s(t)]\}dt \tag{6}$$

where the slug volume, Vol_s, and the contact area between the concentrated liquid layer at the wall and slug, A_{f-s}, can be calculated from measured values of unit cell volume, bubble volume, from slug length L_s and film thickness δ_f. The value of A_{f-s} is expressed as $2\pi r_bL_{f-s}$ or $2\pi r_b(1-\varepsilon_L)L_{UC}$, where ε_L is defined as the ratio between the length of lubrication film (along the bubble) and the unit cell, L_{f-b}/L_{UC} (see Fig. 1).

As shown in Fig. 1, in the present work the film consists of the thin layer at the tube wall along the whole unit cell. It is fed by mass transfer from the bubble lateral interface, and connected to previous and next liquid film layers by a flowrate q_f. Its local dissolved gas concentration, $C_f(z)$, can therefore be

evaluated via the following balance equation established over a small distance dz along the channel:

$$q_f C_f(z+dz) = q_f C_f(z) + \{(k_L)_{f-b} a_{f-b}[C^* - C_f(z)] - (k_L)_{f-s} a_{f-s}[C_f(z) - C_s(z)]\} dz \quad (7)$$

The coefficient $(k_L)_{f-b}$ is expressed following the model of Van Baten and Krishna (2004) by

$$(k_L)_{f-b} = \frac{2}{\sqrt{\pi}} \sqrt{\frac{D u_{TP}}{L_{f-b}}} \quad (8)$$

where a_{f-b} and a_{f-s} are the contact areas between film and bubble, and film and slug, per unit length of the channel respectively. As dz is small compared to L_{UC}, the considered element of film (of length dz), depending on its position z, can be located either close to a bubble or close to a slug. Therefore it is necessary that a_{f-b} is expressed as $2\pi r_b \varepsilon_L$ and a_{f-s} as $2\pi r_b(1-\varepsilon_L)$. Following Svetiov and Abiev (2015), the value of q_f was estimated across film thickness δ_f by locally integrating the liquid velocity profile in the slug, which, as mentioned earlier, is known to conform to the Poiseuille law:

$$q_f = 2\pi \int_{r_b}^{r_c} u(r) r \, dr \quad (9)$$

where

$$u(r) = 2u_{TP}\left[1 - \left(\frac{r}{r_c}\right)^2\right] \quad (10)$$

From the two coupled Eqs. (6) and (7), the evolution of dissolved gas concentrations C_f and C_s along the channel can be computed with initial values $C_f(z=0) = C_s(z=0) = 0$. The resulting dissolved gas concentration in the unit cell, C_{UC}, is simply calculated as the weighted sum of C_s and C_f:

$$Vol_{UC} C_{UC} = Vol_f C_f + Vol_s C_s \quad (11)$$

4. Materials and methods

The two optical techniques used to study the mass transfer in the channel are Planar Laser-Induced Fluorescence with Inhibition (PLIF-I) and shadowgraphy. Both techniques are non-intrusive. Shadowgraphy is a well-known technique which involves illuminating the subject of study by a diffuse light source and recording images of its shadow (Settles, 2001). The basic principle of the PLIF-I technique lays on the excitation of a fluorescent dye by light at a specific wavelength which the dye absorbs. The dye then emits light at a different wavelength and varying intensities due to different inhibiting factors, such as the presence of dissolved molecular oxygen (Dani et al., 2007). When rigorously applied, this technique allows the capture of images of the dissolved gas concentration field. The PLIF-I technique has been used for a decade and can be applied to various gas–liquid systems, like free rising bubbles (Dani et al., 2007; Valiorgue et al., 2013; Häber et al., 2015; Jimenez et al., 2013a) or confined interfaces (Roudet, 2008; Jimenez et al., 2013b). However, the signal to noise ratio may be poor if the laser does not excite the dye at an optimised wavelength. Furthermore, incident and fluorescence lights may be reflected on wall and bubble interface, leading to data processing difficulties and non-negligible uncertainties.

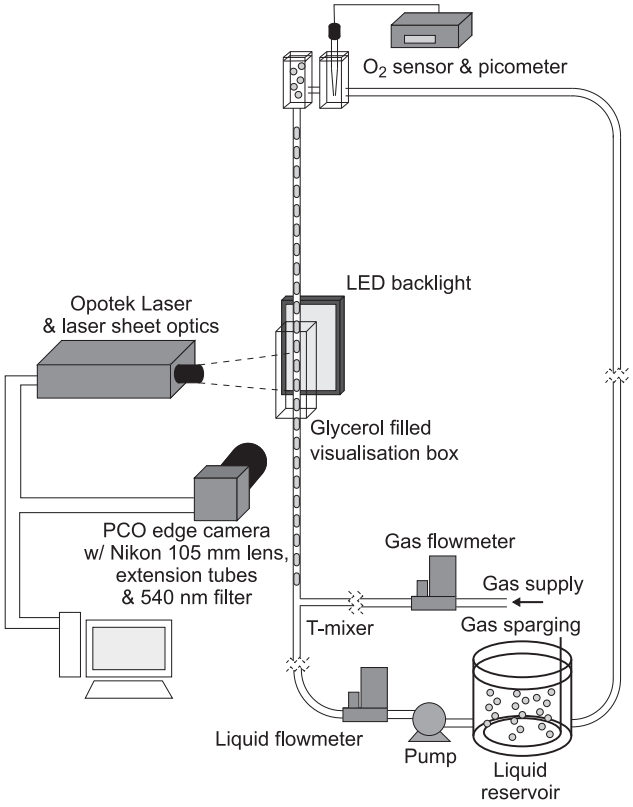

Fig. 2 – Experimental set-up.

In this work, the laser wavelength has been adjusted to the dye excitation spectrum, and a specific data processing has been developed to take light scattering into account. General and specific principles of the techniques are described in the next sections.

4.1. *Experimental test-rig*

The mono-channel is a calibrated glass tube with a circular cross-section and has an internal diameter of 3 mm ± 0.01 mm. The gas is injected into the liquid through a T-mixer located at the channel inlet. It can be set-up so that the inlet can be either at the top or bottom of the channel to allow ascending or descending con-current flows to be generated. The gas flow rate is regulated by a Brooks SLA5850S mass flow meter connected to a West 6100+ digital controller. The liquid phase, consisting of water and dissolved dye, is supplied from a 20 L reservoir tank and is circulated in a closed loop by a Tuthill D-series gear pump with the flow rate regulated by a Bronkhorst CORI-FLOW mass flow controller. The gas and liquid are separated at the outlet. The gas is exhausted to ambient and the liquid returns to the reservoir tank. A gas injection sparging system is included in the liquid reservoir tank. This enables the liquid to be deoxygenated by nitrogen, or given a known oxygen concentration for PLIF-I calibration, described later in Section 4.3. A schematic representation of the setup is shown in Fig. 2.

During the mass transfer experiments, either oxygen or nitrogen was used as the gas phase in the channel, and nitrogen gas is sparged into the liquid reservoir to remove any dissolved oxygen present before it enters the channel. The oxygen concentration at the outlet of the channel is measured by a Unisense OX-50 micro sensor connected to a Unisense

Table 2 – Liquid phase physical properties at 21 °C.	
Density (kg/m^3)	998
Dynamic viscosity (mPa s)	1.05
Surface tension with air (mN/m)	71.2
Henry's constant (mol/m^3/Pa) (Sander, 2015)	1.22×10^{-5}
Mass diffusivity (m^2/s) (Han and Bartels, 1996)	1.77×10^{-9}

PA2000 amplifier. This sensor was used to measure the total mass transfer along the channel length.

4.2. *Imaging and laser systems*

The camera used for the PLIF-I and shadowgraphy imaging was a PCO Edge 5.5 sCMOS camera whose resolution has been reduced to 2560 × 402 pixels to image the channel area of interest only and to enable a higher frequency of acquisition. It is fitted with a Nikon 105 mm Macro f/2.8 lens and extended with a series of extension tubes with a total length of 68 mm. A 540 nm OD 6 high-pass filter is placed in front of the camera.

For the shadowgraphy experiments, a 120 × 160 mm Phlox LED panel is used as the light source. It is positioned behind the channel, perpendicular to the axis of the camera. The imaged section of channel is surrounded by a glycerol filled visualisation box. As the refractive indices of glycerol and glass are almost identical, any refraction or reflection of light as it passes through the channel walls becomes negligible (Schröder and Willert, 2008). The camera acquires images at a frequency of 100 Hz and with an exposure time of 100 μs, effectively freezing the flow.

The light source used for the PLIF-I experiments is an Opotek Opolette 355 tunable laser system. The advantage of using this system is that it can generate wavelengths over a broad range and thus allows for the tuning of the laser light to the maximum excitation wavelength of the PLIF-I dye being used. The dye used in these experiments is Dichlorotis (1,10-phenanthroline) ruthenium(II) hydrate ($C_{36}H_{24}Cl_2N_6Ru{\cdot}xH_2O$) [CAS No. 207802-45-7]. By exciting it at its maximum absorption wavelength (λ_{max} = 450 nm, E = 5 mJ), the resulting emission is maximised and an image with an excellent dynamic range is produced. During this study, it has been verified that images produced using the Opolette laser have a dynamic range approximately 3 times greater than those produced while using a frequency doubled Nd:Yag laser (λ = 532 nm, E = 200 mJ). The 540 nm filter installed on the camera is designed to block the light at the laser wavelength but allow the resulting light at the fluorescence wavelengths to pass. The dye is directly soluble in the aqueous phase and is used at a low concentration of 50 mg/L. As a consequence, it does not significantly alter the liquid phase properties, which have been specifically measured or calculated for this study (see Table 2), and presents constant calibration parameters (Jimenez et al., 2014). Additional tests also showed that there was no photobleaching of the fluid during experiments.

The laser system is equipped with a lens system which produces a diverging laser sheet with a thickness of 280 μm which was measured in-situ. The laser light sheet is positioned to pass through the centerline of the channel and perpendicular to the axis of the camera. A motorised variable attenuator ensures stability of the laser energy pulses. The standard deviations in gray level intensity values show, for three individual pixels in a sequence of concentration calibration images, a time variation of less than 5% from the mean.

For the PLIF-I images, the camera acquisition is triggered by the laser. The camera acquires images at a frequency of 20 Hz and with an exposure of 100 μs, with the camera frequency of acquisition limited by the maximum repetition rate of the laser system.

4.3. *Experimental procedure*

The presented tests were performed at 21 °C and 101.325 kPa respectively. Four oxygen concentration values along the channel length can be quantified: one at the inlet, another at the outlet (using the oxygen sensor), and two at intermediate positions (using PLIF-I technique).

The recorded data allowed the complete processing of four Taylor flow regimes, among them three in the ascending configuration and one in the descending configuration. Their corresponding gas and liquid phase superficial velocities are presented in Table 3, together with their major characteristics.

For each flow regime, sequences of 5000 shadowgraphy and PLIF-I images are recorded. Furthermore, for the same regime, an additional 5000 shadowgraphy and PLIF-I images are recorded using nitrogen bubbles in place of oxygen bubbles. As the liquid phase entering the channel is deoxygenated by nitrogen during the experiments, no mass transfer takes places between the liquid and nitrogen gas bubbles and there is therefore no dye quenching. These images are used as reference images in the image processing stage described in Section 4.4.

For the imaging of a certain Taylor flow regime, the experimental set-up allows for the shadowgraphy and PLIF-I experiments to be conducted directly one after the other without any movement of equipment or disturbance of the flow in the channel. It is simply necessary for the required light source to be activated and the camera set to the corresponding frequency of acquisition to record images with different dynamic ranges.

At each position along the channel, calibrations are also acquired so the image intensity gray values can be related to the oxygen concentration. Since oxygen molecules inhibit dye fluorescence (Jimenez et al., 2014), their presence in a liquid phase can easily be tracked and quantified based on the Stern–Volmer relation:

$$\frac{I_0(x,y)}{I(x,y)} = 1 + K_{SV}(x,y) \cdot [O_2](x,y) \tag{12}$$

where x and y are the coordinates of the considered pixel in the image, I is a pixel gray value at a certain O_2 concentration $[O_2]$, I_0 is a pixel gray value in the absence of O_2, and K_{SV} is the Stern–Volmer constant. The calibration procedure involves saturating the liquid at known oxygen concentration values and recording the resulting fluorescence received by the imaging system (Dani et al., 2007). The five concentration values for the oxygen-nitrogen gas mixtures used were 0%, 5%, 10%, 21% and 100% (in oxygen). For a given concentration value, 100 images are used to create a time-averaged image. The value of K_{SV} can then be determined by a linear regression fit of the data, pixel-by-pixel. This type of calibration procedure therefore accounts for laser sheet non-uniformity, absorption, pixel response non-uniformity, and lens vignette (Webster et al., 2001; Valiorgue et al., 2013).

Table 3 – Recorded Taylor flow regimes and their major characteristics.

Regime	u_{GS} (m/s)	u_{LS} (m/s)	u_{TP} (m/s)	u_b (m/s)	L_{UC} (mm)	L_s (mm)	Vol_b (mm^3)	ε_L (%)	δ_f (μm)	Axial position of PLIF-I	
										z_1 (m)	z_2 (m)
1 (desc.)	0.056	0.161	0.217	0.240	10.2	9.63	16.8	5.6	43	0.595	0.93
2	0.103	0.143	0.247	0.283	12.7	9.89	33.2	22.7	55	0.245	0.625
3	0.045	0.079	0.124	0.140	15.8	12.50	36.4	20.8	46	0.195	0.505
4	0.222	0.118	0.339	0.395	9.7	5.90	38.7	39.3	112	0.195	0.505

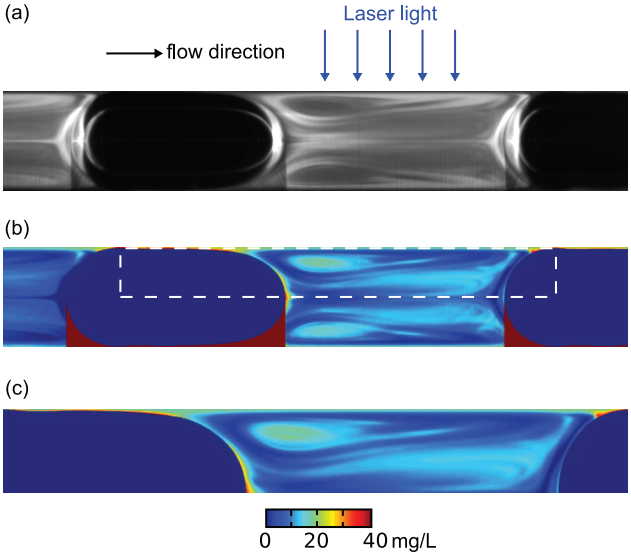

Fig. 3 – PLIF-I images of recorded regime 2 (see Table 3) at z = 0.245 m (t = 0.99 s): (a) instantaneous gray value image; (b) corresponding instantaneous [O_2] image; (c) corresponding time-averaged [O_2] unit cell half-image.

4.4. *Image processing*

In order to extract the quantitative data related to the mass transfer taking place between the two phases, significant processing of the images is required. The processing includes a number of edge detection, calibration and correction steps, and is described in detail in Butler et al. (2016). The processing is realised with a self-developed MATLAB code. Computationally intensive tasks are performed on a graphics processing unit (GPU) by integrating custom CUDA kernels.

The application of the image processing on the shadowgraphy images leads to the determination of channel wall position, bubble interface, bubble radius, bubble and slug lengths, and bubble average velocity.

For the correction of light scattering effects, two series of PLIF-I images are recorded using the same flowrates: one series obtained with N_2 bubbles (no mass transfer between liquid and gas, no fluorescence quenching) and the other series obtained with O_2 bubbles (showing quenching due to mass transfer). The most frequent slug length, i.e. the mode, is calculated from the combined O_2 and N_2 images. This value is used to ensure that a maximum number of instantaneous images (at least 100) can be used to create time-averaged images in which all the slug lengths are exactly the same. Before creating the time-averaged O_2 images however, the instantaneous images are first converted from gray values to [O_2]. For this, Eq. (12) is used as the K_{SV} calibration described in Section 4.3 is designed to work pixel-by-pixel. Fig. 3(a) and (b) show an instantaneous gray value image recorded by the camera and the resulting image converted into [O_2], respectively. Fig. 3(c) shows the corresponding time-averaged [O_2] unit cell image. The [O_2] image colour scale ranges from 0 to 39.524 mg/L. This maximum value C^* is the theoretical saturation [O_2] calculated from Henry's law (Henry's constant is given in Table 2).

In Fig. 3(a) and (b), the data hidden by the bubble shadow cannot be exploited (lower half of figures). However, the unit cell is expected to be axisymmetrical about the channel axial centreline. To calculate the total mass of dissolved O_2 in the liquid phase, an integration of the [O_2] in the half unit cell (Fig. 3(c)) is performed around the axial centreline. The volumes of discs corresponding to each pixel revolved around the axis are calculated using magnification factors determined from a spatial calibration step.

The liquid phase is then separated into the slug and film areas in order to determine the individual contributions of the film and bubble caps to the total mass of dissolved O_2. The film is defined as the thin region along the channel wall and the slug is the remaining liquid phase. Fig. 4 shows the unit cell for regime 2: the dashed line defines the film boundary. Between the bubble and channel wall, the gas–liquid interface defines the location of the film. In the slug zone, the film location is determined by detection of the locations of the maximum gradient of [O_2] close to the wall.

5. Results and discussion

5.1. *Geometrical and operational flow characteristics*

For the four recorded Taylor flow regimes (one descending and three ascending), geometrical and operational values are determined from the shadowgraphy images and are shown in Table 3. It can be observed that the data shows contrasted values of bubble velocity u_b (0.14–0.40 m/s), two-phase superficial velocity u_{TP} (0.12–0.34 m/s), slug length (5.9–12.5 mm) and bubble volume (16.8–38.7 mm^3), leading to contrasted values of the gas holdup ε_L in the unit cell. Film thickness varies in the range 43–112 μm.

The film thickness δ_f is calculated as the average thickness between the bubble and channel wall where the bubble interface angle relative to the channel wall was between ±5°. For the first three recorded regimes, the film thickness is found to be 55 μm, 43 μm and 46 μm respectively. These values are found to be within 10 μm when compared to the relationship of Aussillous and Quéré (2000) for relatively high Capillary number ($Ca \sim 0.003$). For the fourth regime, showing very short slugs, a significant difference is observed between measurement (112 μm) and prediction (58 μm). Some of the difference may be due to the fact that this relationship was derived for bubbles with long lubrication films (5–10 cm) of constant thickness, which is not the case for the regimes presented here. Furthermore, due to the increased effect of refraction close to the tube, the uncertainty of the film thickness is relatively high

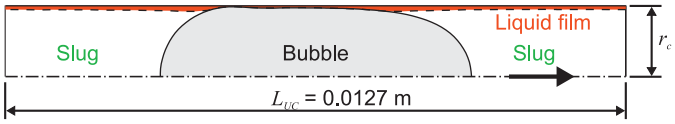

Fig. 4 – Measured film boundary for regime 2.

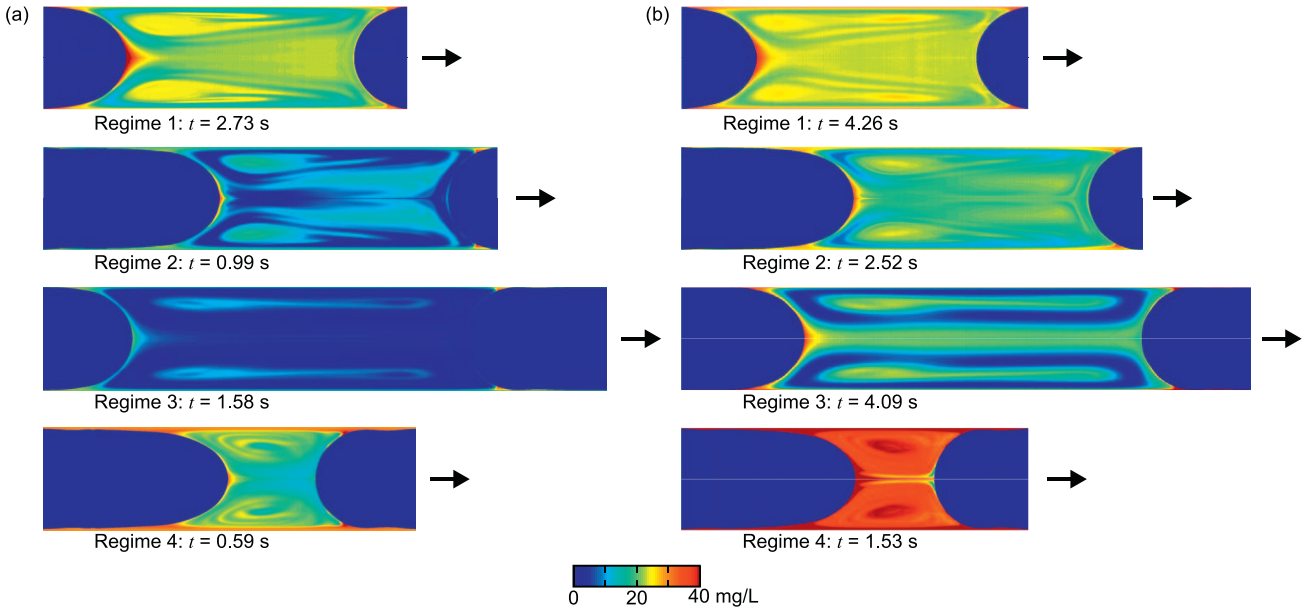

Fig. 5 – Time-averaged PLIF-I images of recorded regimes at different travelling times t: (a) First axial position; (b) Second axial position. The upper unit cell image is mirrored about the axial centreline.

as each pixel in this region is equal to approximately 11 μm. The film is approximately 3–6 pixels wide.

5.2. *Time-averaged concentration fields*

Fig. 5 presents the time-averaged [O_2] images for each of the four recorded Taylor flow regimes, at two axial positions along the channel. The images are presented with a common scale so that the difference in flow characteristics (unit cell length, bubble length, etc.) can be clearly visualised. It is worth highlighting that the unit cell, and the slug itself, are not uniform in concentration. The zones of greatest [O_2] are visible in front of the bubble nose and along the channel wall (i.e. in the film). The effect of slug recirculation on concentration distribution is clearly observed. The observed patterns of oxygen iso-concentration areas are very similar to the patterns computed with CFD by Hassanvand and Hashemabadi (2012) for millimetric capillaries. However, some differences include the areas rich in dissolved oxygen in the central part of slug vortices, which are not observed in CFD concentration fields.

As expected, in all cases, the overall [O_2] increases with time. It is interesting to note that for regime 4, corresponding to the highest u_{TP} and the smallest L_s, the average concentration in O_2 almost reaches saturation in a short travelling time.

5.3. *Mass transfer evolution along the channel*

For each recorded Taylor flow regime, the mean concentration of dissolved O_2 in the liquid phase is measured at the channel outlet. In Table 4, these values are presented in terms of achieved mass transfer relative to complete saturation of the unit cell in dissolved O_2, and the relative contribution of films to the achieved mass transfer is extracted from the processing of the PLIF-I images at z_2 (Fig. 5(b)).

It is clearly evident that mass transfer between gas and liquid phases in Taylor flow is the most efficient when the u_{TP} is high and when L_s is short (regime 4). It can also be observed that film contribution to overall mass transfer remains moderate (less than 40%). This may be explained by the short length of film which is in contact with the bubble (less than 4 mm), in all of the four investigated Taylor flow regimes. Film-bubble contact times exceed the diffusive criterion ($0.1\delta_f^2/D$) from Van Baten and Krishna (2004) by a factor of at least 15. The weakest film contribution (21%) to the overall mass transfer corresponds to the shortest contact length (0.57 mm for regime 1).

The evolution of concentration of dissolved O_2 along the tube and at channel outlet (measured from the oxygen probe), are shown in Fig. 6: the mean concentrations in the unit cell, film, and slug are normalised by C^*, and plotted at their corresponding axial positions z (from tube inlet). The error bars presented in Fig. 6 for the PLIF-I measurements are estimated on the basis of the maximum fluctuation of the pixel gray values that have been used to create the time-averaged images. The resulting uncertainty was determined to be approximately ±3%. However, this value is probably higher for the PLIF-I measurements made in the lubrication films, because of the increased distortion effect in the vicinity of the tube wall, and of the restricted number of pixels to describe the film area. The latter point makes the uncertainty for film concentration difficult to quantify. For the probe measurements, the uncertainty was found to be approximately ±4%.

Concerning overall [O_2] in the unit cell, the PLIF-I and probe measurements are seen to be in good agreement. The slope of the curve is greater at lower values of z and reduces

Table 4 – Recorded Taylor flow regimes and their major characteristics in terms of achieved mass transfer at channel outlet.

Regime	u_{TP} (m/s)	L_{f-b} (mm)	Achieved mass transfer (%, $C^* = 39.5$ mg/L)	Film contribution for z_2 (%)	Slug residence time at z_2 (s)
1	0.22	0.57	73	21	4.3
2	0.25	2.91	73	28	2.5
3	0.12	3.29	69	25	4.1
4	0.34	3.8	>99	38	1.5

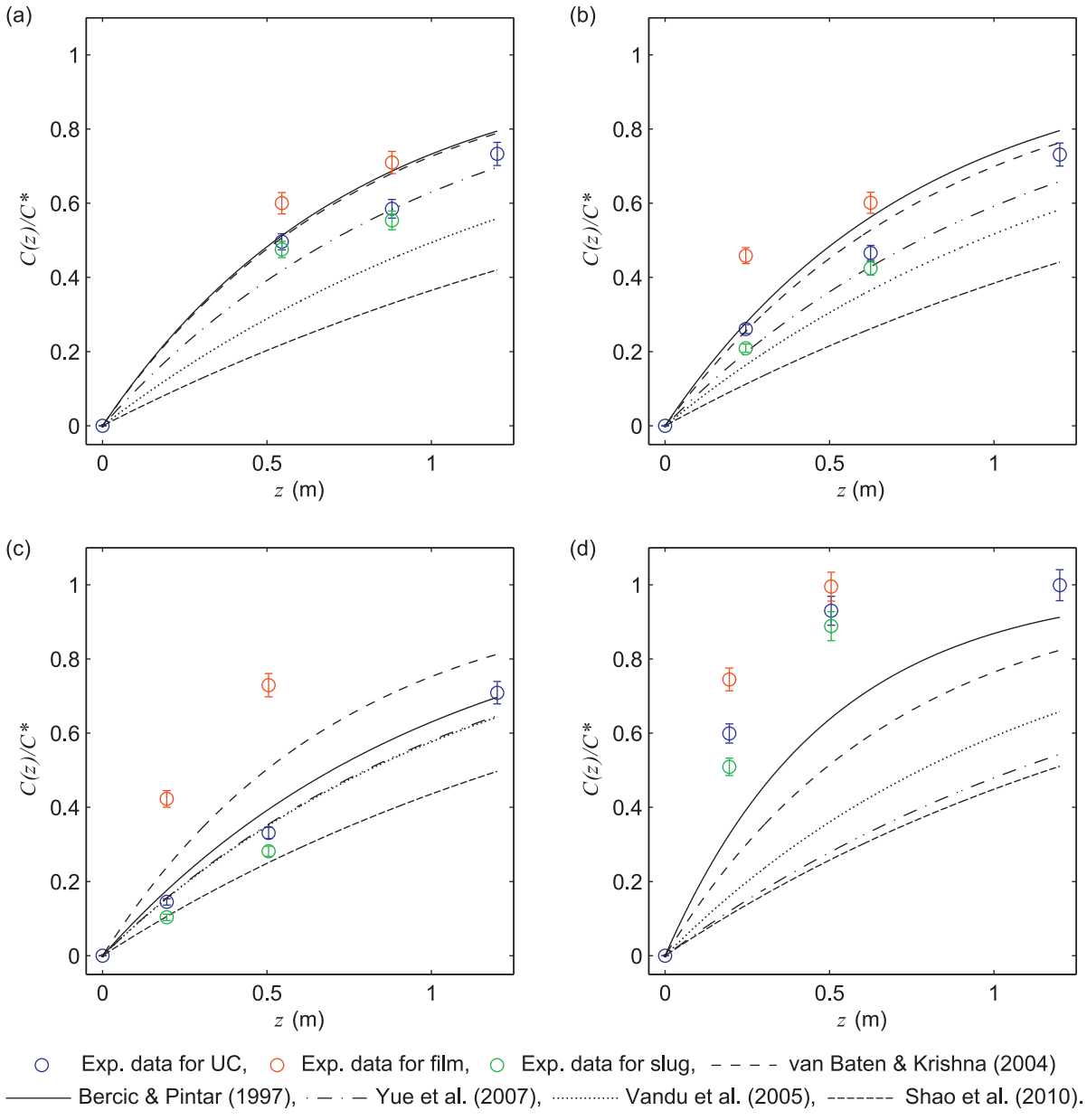

Fig. 6 – Evolution of dissolved O_2 concentration along the channel compared to literature models: (a) Regime 1; (b) Regime 2; (c) Regime 3; (d) Regime 4.

significantly as the flow travels along the channel, indicating that a high proportion of the mass transfer occurs close to the inlet. At the outlet, the liquid is often not yet fully saturated (except for regime 4). Oxygen concentrations in films, which have been experimentally measured for the first time, clearly outweigh concentrations in slugs. However, even if films enrich faster than slugs, their contribution to overall mass transfer is moderate for regimes 1 to 3 because of their small volumes (for these cases, Vol_f /Vol_s ranges from 12% to 28%, whereas it reaches 58% for regime 4), and because their contact length with bubbles, L_{f-b}, are short, as shown in Table 4.

5.4. *Models for mass transfer in Taylor flow*

The experimental values of overall [O_2] in the unit cell are used to test the k_La models presented in Table 1, which are based on the assumption of plug flow. For regimes 1 and 2, Fig. 6(a) and (b) show that the model from Yue et al. (2007) is in good agreement with the experimental data (with respective k_La values of 0.215 s^{-1} and 0.220 s^{-1}), and that the models from Van Baten and Krishna (2004), Berčič and Pintar (1997), and to a lesser extent Vandu et al. (2005), give satisfying tendency for the evolution of concentration along the channel.

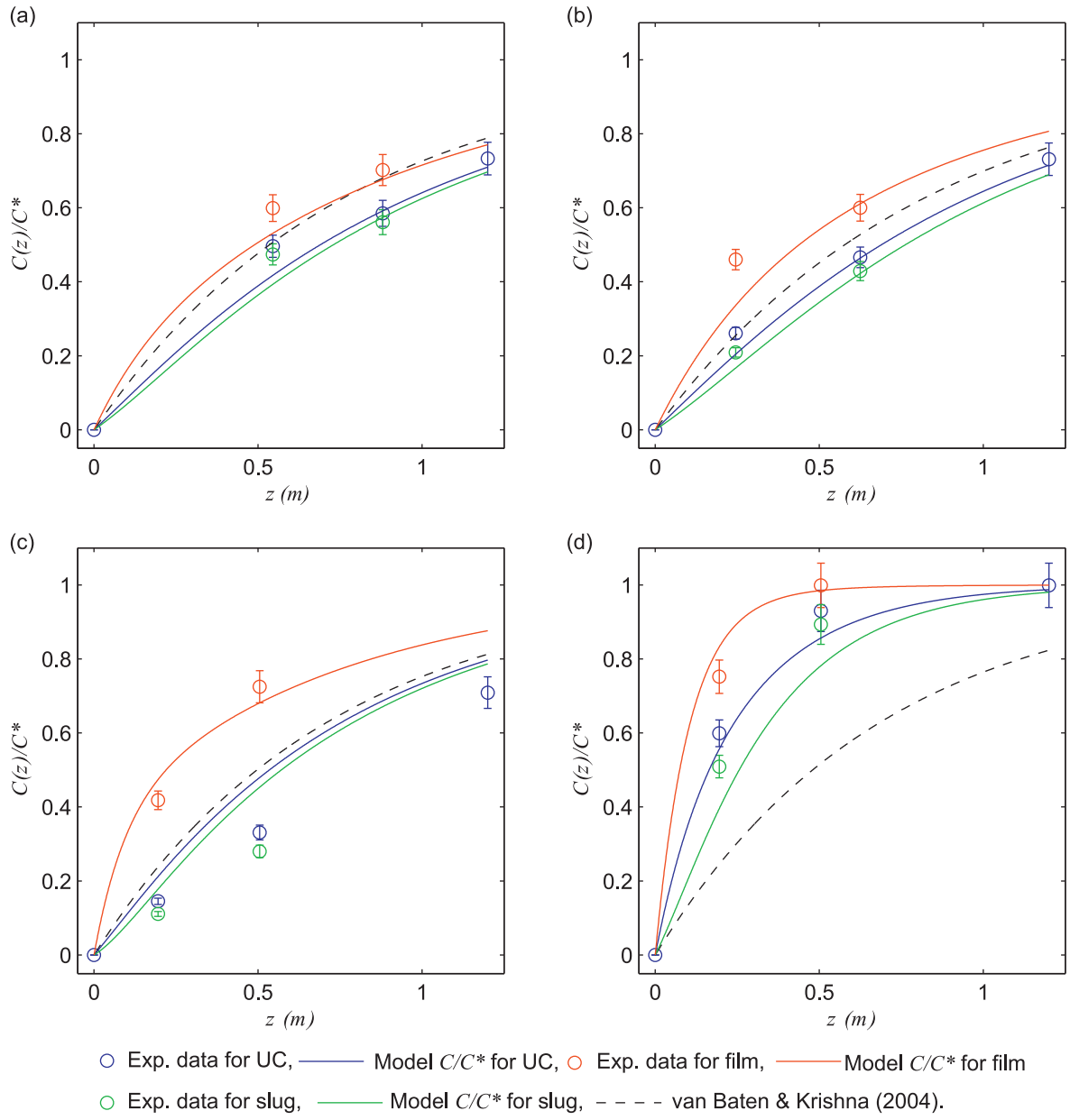

Fig. 7 – Comparison of the proposed model of separate additive contributions to local experimental data acquired by PLIF-I technique: (a) Regime 1; (b) Regime 2; (c) Regime 3; (d) Regime 4.

For regime 3 however (long slugs, Fig. 6(c)), model from Van Baten and Krishna (2004) over-estimates mass transfer. Model from Shao et al. (2010) does not fit the data. For regime 4 (short slugs, Fig. 6(d)) all the tested models clearly under-estimate the rate of mass transfer. We recall that these models do not consider the actual structure of the flow, even the model from Van Baten and Krishna (2004) where film and caps contributions are distinguished but then merged into a single k_La coefficient, regardless of local gradients in concentrations.

The consideration of the separate mass transfer mechanisms (Eqs. (4)–(11)) allows one to follow the evolution of the various local concentrations, as well as the overall unit cell concentration (Fig. 7). The flow characteristics required to calculate all the parameters used in these equations are d_c, u_{TP}, L_s, L_{f-b}, L_{UC}, and δ_f. They have been measured with the shadowgraphy technique only and are reported in Tables 3 and 4. As mentioned earlier, values of $(k_L)_{f-b}$ and $(k_La)_{caps}$ used in the model are calculated in a similar way to that proposed in the model of Van Baten and Krishna (2004) (Eq. (B2)), other than the use of u_{TP} in place of u_b.

Fig. 7 shows that the model of separate additive contributions satisfactorily fits the experimental data: this model predicts the evolution of the unit cell concentration along the channel for the four recorded regimes. In particular, the fast increase of gas concentration at channel entrance in the case of short slugs (regime 4, Fig. 7(d)) is well reproduced by the model, whereas the models based on plug flow are unable to describe $[O_2]$ evolution for regime 4 (see the model of Van Baten and Krishna (2004) shown in Fig. 7(d)). What is more, the evolutions of film and slug concentrations are also well reproduced by the separate additive contribution model.

As expected, the model is sensitive to the values of $(k_L)_{f-b}$, $(k_La)_{caps}$, and q_f, and to a lesser extent $(k_L)_{f-s}$. It is however important to note that, to fit the experimental data, it was necessary (i) to divide $(k_L)_{f-b}$ by a factor of 35 and $(k_La)_{caps}$

Table 5 – Mass transfer coefficients used in the model of separate additive contributions.

	$(k_L a)_{caps}$ (1/s)	$(k_L)_{f-b}$ (m/s)	$(k_L)_{f-s}$ (m/s)
$L_s < 2d_c$	$\frac{2\sqrt{2}}{\pi}\sqrt{\frac{Du_{TP}}{d_c}}\frac{4}{L_{UC}}$	$\frac{2}{3.5\sqrt{\pi}}\sqrt{\frac{Du_b}{L_{f-b}}}$	$\frac{3.66D}{d_c}$
$L_s > 2d_c$	$\frac{2\sqrt{2}}{1.8\pi}\sqrt{\frac{Du_{TP}}{d_c}}\frac{4}{L_{UC}}$	$\frac{2}{3.5\sqrt{\pi}}\sqrt{\frac{Du_b}{L_{f-b}}}$	

by a factor of 1.8 for regimes 1 to 3 (long slugs), and (ii) to divide $(k_L)_{f-b}$ by a factor of 3.5 for regime 4 (short slugs). This shows that the contribution of films derived by Van Baten and Krishna (2004) in Eq. (8) is greatly over-estimated for the regimes with long slugs ($L_s > 2d_c$), as well as for regimes with long film-bubble contact times ($\tau_f > 1.5\delta_f^2/D$). This may be explained by the order of magnitude of the velocity used in this equation, i.e. either u_{TP} or u_b, thus considering stagnant film at the wall, whereas velocities in the film may be non-negligible, especially in the case of contaminated bubble surface. Further measurement of additional regimes and local investigation by means of Computational Fluid Dynamics should permit the full determination of this effect. Table 5 summarises the equations for determination of the mass transfer coefficients used in the model of separate additive contributions.

6. Conclusions

Mass transfer taking place in Taylor flow in a millimetric channel has been successfully quantified. It is the first time the PLIF-I technique has been implemented to study this phenomenon. This technique has allowed for the measurement of the local gas concentration in the liquid slugs and films. Mass transfer between gas and liquid phase was found to be the most efficient for short slugs and high total superficial velocity. Among several available mass transfer models, a relation estimating the overall volumetric mass transfer coefficient $k_L a$ from the contributions of films and caps to mass transfer, published by Van Baten and Krishna (2004), was found unable to accurately describe the experimental results in the case of small slugs (in this study: $L_s < 2d_c$). In the present work, an improved model was proposed: as the major geometric and dynamic characteristics of the flow were known thanks to shadowgraphy measurements, it was possible to derive the actual separate contributions by taking into account interfacial mass transfer towards film and slug (on the basis of the relations suggested by Van Baten and Krishna (2004) for estimation of the respective mass transfer coefficients), and mass exchange between film and slug. This method gives satisfying results regarding overall dissolved gas concentration in the channel, and also allows for a very good estimation of dissolved gas concentrations in films and slugs. It has been further shown that the interfacial mass transfer between bubble and film $(k_L)_{f-b}$ is over-estimated by the relation derived by Van Baten and Krishna (2004) and needs to be adapted by use of a correction factor (as presented in Table 5).

In future work, more Taylor flow regimes will be investigated, showing contrasted geometrical and dynamical characteristics. Regimes with long bubbles will be of particular interest to emphasise film contribution to mass transfer. In order to estimate more accurately the film contribution for the model of separate additive contributions, the order of magnitude of the liquid velocity in the film will be investigated via CFD calculations.

Nomenclature

A	contact area (m^2)
a	contact area per volume of unit cell or per unit length of channel (m^2/m^3, m^2/m)
C	dissolved gas concentration (mg/L)
C^*	dissolved gas saturation concentration (39.524 mg/L)
Ca	Capillary number (–)
D	mass diffusivity (m^2/s)
d	diameter (m)
I	pixel gray value intensity (–)
K_{SV}	Stern–Volmer coefficient (L/mg)
k_L	liquid phase mass transfer coefficient (m/s)
L	length (m)
q	volumetric flowrate (m^3/s)
Re	Reynolds number (–)
r	radius (m)
Sc	Schmidt number (–)
Sh	Sherwood number (–)
t	time (s)
u	velocity (m/s)
u_{GS}, u_{LS}	superficial velocity (m/s)
Vol	volume (m^3)
x, y	pixel coordinates
z	axial distance from channel inlet (m)

Greek

δ	thickness (m)
$\varepsilon_L = L_{f-b}/L_{UC}$	length void fraction (–)
$\varepsilon_V = Vol_b/Vol_{UC}$	volume void fraction (–)
τ	contact time (s)

Subscripts

b	gas bubble
c	channel
$caps$	bubble caps
f	liquid lubrication film
$f-b$	liquid lubrication film between bubble and channel wall
$f-s$	liquid lubrication film between liquid slug and channel wall
G	gas phase
L	liquid phase
TP	two phase
s	liquid slug
UC	unit cell

Acknowledgments

The authors thank the Agence National de la Recherche (ANR) for financial support, and the Fédération de Recherche FERMaT for financial and technical support.

References

Abiev, R., 2013. Bubbles velocity, Taylor circulation rate and mass transfer model for slug flow in milli- and microchannels. Chem. Eng. J. 227, 66–79.

Aussillous, P., Quéré, D., 2000. Quick deposition of a fluid on the wall of a tube. Phys. Fluids 12 (10), 2367–2371.

Berčič, G., Pintar, A., 1997. The role of gas bubbles and liquid slug lengths on mass transport in the Taylor flow through capillaries. Chem. Eng. Sci. 52 (21), 3709–3719.

Butler, C., Cid, E., Billet, A.-M., 2016. Investigation par inhibition de fluorescence des mécanismes locaux de transfert de masse en écoulement de Taylor. In: Proceedings of Congrès Francophone de Techniques Laser, Toulouse, France, 13–16 September 2016.
Dani, A., Guiraud, P., Cockx, A., 2007. Local measurement of oxygen transfer around a single bubble by planar laser-induced fluorescence. Chem. Eng. Sci. 62, 7245–7252.
Das, S., 2010. Fundamentals of Heat and Mass Transfer. Alpha Science International Ltd., Oxford, UK.
Dietrich, N., Loubière, K., Jimenez, M., Hébrard, G., Gourdon, C., 2013. A new direct technique for visualizing and measuring gas–liquid mass transfer around bubbles moving in a straight millimetric square channel. Chem. Eng. Sci. 100, 172–182.
Häber, T., Gebretsadik, M., Bockhorn, H., Zarzalis, N., 2015. The effect of total reflection in PLIF imaging of annular thin films. Int. J. Multiph. Flow 76, 64–72.
Han, P., Bartels, D., 1996. Temperature dependence of oxygen diffusion in H_2O and D_2O. J. Phys. Chem. 100, 5597–5602.
Hassanvand, A., Hashemabadi, S.H., 2012. Direct numerical simulation of mass transfer from Taylor bubble flow through a circular capillary. Int. J. Heat Mass Transf. 55, 5959–5971.
Hatziantoniou, V., Andersson, B., Schoon, N.H., 1986. Mass transfer and selectivity in liquid-phase hydrogenation of nitro compounds in a monolithic catalyst reactor with segmented gas–liquid flow. Ind. Eng. Chem. Process Des. Dev. 25 (4), 964–970.
Heiszwolf, J.J., Kreutzer, M.T., van den Eijnden, M.G., Kapteijn, F., Moulijn, J.A., 2001. Gas–liquid mass transfer of aqueous Taylor flow in monoliths. Catal. Today 69 (1–4), 51–55.
Incropera, F.P., DeWitt, D.P., 2002. Fundamentals of Heat and Mass Transfer, 5th ed. John Wiley & Sons, New Jersey, USA.
Irandoust, S., Ertlé, S., Andersson, B., 1992. Gas–liquid mass transfer in Taylor flow through a capillary. Can. J. Chem. Eng. 70, 115–119.
Jimenez, M., Dietrich, N., Grace, J.R., Hébard, G., 2014. Oxygen mass transfer and hydrodynamic behaviour in wastewater: determination of local impact of surfactants by visualization techniques. Water Res. 58, 111–121.
Jimenez, M., Dietrich, N., Hébrard, G., 2013a. Mass transfer in the wake of non-spherical air bubbles quantified by quenching of fluorescence. Chem. Eng. Sci. 100, 160–171.
Jimenez, M., Dietrich, N., Hébrard, G., Cockx, A., 2013b. Experimental study of O_2 diffusion coefficient measurement at a planar gas–liquid interface by planar laser-induced fluorescence with inhibition. AIChE J. 59, 325–333.
Kececi, S., Wörner, M., Onea, A., Soyhan, H.S., 2009. Recirculation time and liquid slug mass transfer in co-current upward and downward Taylor flow. Catal. Today 147, S125–S131.
Kreutzer, M.T., Du, P., Heiszwolf, J.J., Kapteijn, F., Moulijn, J.A., 2001. Mass transfer characteristics of three-phase monolith reactors. Chem. Eng. Sci. 56 (21), 6015–6023.
Liu, D., Wang, S., 2010. Gas–liquid mass transfer in Taylor flow through circular capillaries. Ind. Eng. Chem. Res. 50 (4), 2323–2330.
Mehdi, S., Billet, A.-M., Chughtai, I.R., Inayat, M., 2013. Overall gas–liquid mass transfer from Taylor bubbles flowing upwards in a circular capillary. Asia-Pac. J. Chem. Eng. 8, 931–939.
Nijhuis, T.A., Kreutzer, M.T., Romijn, A.C.J., Kapteijn, F., Moulijn, J., 2001. Monolithic catalysts as efficient three-phase reactors. Chem. Eng. Sci. 56 (3), 823–829.
Pan, Z., Zhang, X., Xie, Y., Cai, W., 2014. Instantaneous mass transfer under gas–liquid Taylor flow in circular capillaries. Chem. Eng. Technol. 37, 495–504.
Roudet, M., (Ph.D. thesis) 2008. Hydrodynamique et transfert de masse autour d'une bulle confinée entre deux plaques. Université de Toulouse http://ethesis.inp-toulouse.fr/archive/00000806/.
Sander, R., 2015. Compilation of Henry's law constants (version 4.0) for water as solvent. Atmos. Chem. Phys. 15, 4399–4981.
Schröder, A., Willert, C.E., 2008. Particle Image Velocimetry: New Developments and Recent Applications. Springer-Verlag Berlin Heidelberg GmbH, New York.
Settles, G.S., 2001. Schlieren and Shadowgraphy Techniques: Visualizing Phenomena in Transport Media. Springer-Verlag Berlin Heidelberg GmbH, New York.
Shao, N., Gavriilidis, A., Angeli, P., 2010. Mass transfer during Taylor flow in microchannels with and without chemical reaction. Chem. Eng. Sci. 160 (3), 873–881.
Svetiov, S.D., Abiev, R.S., 2015. Mass transfer in Taylor flow in microchannels: modelling of convection effects. In: Proceedings of 15th European Conference on Mixing, Saint Petersburg, Russia, 28 June–3 July 2015.
Tan, J., Lu, Y.C., Xu, J.H., Luo, G.S., 2012. Mass transfer performance of gas–liquid segmented flow in micro channels. Chem. Eng. J. 181, 229–235.
Thulasidas, T.C., Abraham, M.A., Cerro, R., 1995. Bubble-train flow in capillaries of circular and square cross section. Chem. Eng. Sci. 50 (2), 183–199.
Thulasidas, T.C., Abraham, R.L., Cerro, R.L., 1997. Flow patterns in liquid slugs during bubble-train flow inside capillaries. Chem. Eng. Sci. 52, 2692–2947.
Valiorgue, P., Souzy, N., El Hajem, M., Ben Hadid, H., Simoëns, S., 2013. Concentration measurement in the wake of a free rising bubble using planar laser-induced fluorescence (PLIF) with a calibration taking into account fluorescence extinction variations. Exp. Fluids 54, 1–10.
Van Baten, J.M., Krishna, R., 2004. CFD simulations of mass transfer from Taylor bubbles rising in circular capillaries. Chem. Eng. Sci. 59 (12), 2535–2545.
Vandu, C.O., Ellenberger, J., Krishna, R., 2004. Hydrodynamics and mass transfer in an upflow monolith loop reactor: influence of vibration excitement. Chem. Eng. Sci. 59 (22–23), 4999–5008.
Vandu, C.O., Liu, H., Krishna, R., 2005. Mass transfer from Taylor bubbles rising in single capillaries. Chem. Eng. Sci. 60 (22), 6430–6437.
Webster, D.R., Roberts, P.J.W., Ra'ad, L., 2001. Simultaneous DPTV/PLIF measurements of a turbulent jet. Exp. Fluids 30, 65–72.
Yao, C., Dong, Z., Zhao, Y., Chen, G., 2014. An online method to measure mass transfer of slug flow in a micro channel. Chem. Eng. Sci. 112, 15–24.
Yue, J., Yuan, Q., Luo, L., Gonthier, Y., 2007. Hydrodynamics and mass transfer characteristics in gas–liquid flow through a rectangular microchannel. Chem. Eng. Sci. 62 (7), 2096–2108.